MPS/Int. MA 67-11
AAS/amm - 1.8.1967

Technical Note No. 92

CALCULATION OF EDDY CURRENT EFFECTS IN THE VACUUM CHAMBERS OF THE BOOSTER SYNCHROTRON QUADRUPOLE AND BENDING MAGNETS

by A. Ašner

1. SUMMARY

The magnetic field and field gradient distorsions due to eddy currents in rectangular and elliptic vacuum chambers of the Booster Synchrotron bending magnets and in a circular chamber of the quadrupole lenses have been computed.

The field distorsion in the bending magnet at a main field rise of 7 $\frac{Wb}{m^2 s}$ - 7 kG in 100 ms - corresponding to half of the actual PS energy gain, is important: The maximum relative field error at injection would for a 2 mm stainless steel rectangular or elliptic vacuum chamber amount to - 0,8 o/oo.

The situation in the quadrupole lenses is more convenient : The first order eddy current field is an ideal quadrupolar field. The higher order terms, due to the imaged eddy currents give a relative gradient error at injection of less than -2 o/oo, this at 80 o/o of the aperture.

In order to reduce or compensate the magnetic field errors, the main field rise time should be increased beyond 600 ms. Should this for other reasons not be possible, ceramic vacuum chambers or eddy current compensating d.c. windings could be placed on the bending magnet elliptic or rectangular vacuum chambers, reducing the effective gap by 6 ... 10 mm.

2. EFFECT OF CIRCULAR VACUUM CHAMBER EDDY CURRENTS IN THE BOOSTER QUADRUPOLE LENSES.

We assume a circular vacuum chamber of radius r(m), wall thickness δ (m) and conductivity x (Ω^{-1} m^{-1}) placed in an ideal quadrupolar field $B_o(r)$, g.r ($\frac{Vs}{m^2}$). The field rises linearly in time, so $\frac{dB_o}{dt}$ = const.

Applying in accordance with Fig. 1 Maxwell's equation in cylindric coordinates :

$$\text{rot } \vec{E} = \text{rot } \vec{E}_z = -\frac{\partial B_o}{dt} = \frac{1}{r}\frac{\partial}{\partial r}(r\, B_\varphi) - \frac{1}{r}\frac{dB_r}{d\varphi} \quad \ldots \quad (1)$$

and taking into account that only the B_r - magnetic field component contributes to the creation of eddy currents in the chamber, - see Fig. 1b :

$$\frac{1}{r}\frac{\partial E_r}{\partial \varphi} = \frac{\partial B_o}{\partial t} \sin 2\varphi \quad \ldots \quad (2)$$

The eddy current density is then :

$$j(\varphi) = r \cdot x \cdot \frac{dB_o}{dt} \int_o^\varphi \sin \varphi d\varphi = \frac{-r\, x \frac{dB_o}{dt}}{2} \cos 2\varphi \quad (3)$$

and the eddy current :

$$I(\varphi) = j(\varphi).\delta\, r d\varphi = \frac{-r^2}{2} x\, \delta \frac{dB_o}{dt} \cos 2\varphi\, d\varphi \quad (4)$$

This current will in accordance with Fig. 2 create a magnetic field B_y:

$$B_y = \int_o^\pi - M \frac{\mu_o}{\pi} \frac{(r\cos\varphi - x)\cos 2\varphi}{r^2+x^2-2rx\cos 2\varphi} d\varphi \quad \ldots \quad (5)$$

with

$$M = \frac{r^2}{2} x\, \delta \frac{dB_o}{dt} \quad \ldots \quad (6)$$

After some computation one obtains (1) :

$$B_y = -M \frac{\mu_o}{\pi} \cdot \frac{x}{xr^2} \left[\frac{Vs}{m^2}\right] \quad \ldots \quad (7)$$

and for the gradient :

$$g_{e.c.} = \frac{\partial B_y}{\partial x} = -\frac{x\, \delta\, \mu_o \frac{dB_o}{dt}}{4} \left[\frac{Vs}{m^3}\right] \quad \ldots \quad (8)$$

which corresponds to an ideal quadrupolar field opposed to the lens main field.

Introducing the following numerical values : $\frac{dB_o}{dt} = 2,5 \frac{V}{m^2}$ (2,5 kG in 100 ms), $\delta = 0,002m$, $x = 10^{+6} (\Omega^{-1} m^{-1})$ (stainless steel) one finds :

$$g_{ec.} = 1,5 \cdot 10^{-3} \frac{Vs}{m^3} ; \left(\frac{\Delta g}{g}\right)_{inj} = \frac{1,5.10^{-3}}{1,0} = \underline{\underline{1,5 \text{ o/oo}}}$$

We will now calculate the influence of the imaged eddy current terms. To do this, we use the conformal transformation :

$$w = u + iv = z^2 = (x+iy)^2 \quad \ldots\ldots\ldots\ldots \quad (9)$$

yielding

$$u = x^2 - y^2 \quad \ldots\ldots\ldots\ldots \quad (10)$$

$$v = 2 x y \quad \ldots\ldots\ldots\ldots \quad (11)$$

Fig. 2 shows the imaged eddy current density distribution in the w-plane along a half circle :

$$u^2 + (2v_o - v)^2 = \rho^2 \quad \ldots\ldots\ldots\ldots \quad (12)$$

In accordance with Fig. 3a one obtains for the coordinates of the imaged current in point P_i (u,v)

$$u = x'^2 - y'^2 = \rho \cos\psi \quad \ldots\ldots\ldots\ldots \quad (13)$$

$$v = 2x' y' = 2v_o - \rho \sin\psi \quad \ldots\ldots\ldots\ldots \quad (14)$$

From eq. 13 and 14 the corresponding real plane coordinates x', y' of the imaged eddy current part can be found for different values of ψ ($o<\psi<90^o$).

Fig. 3b shows the obtained location of the imaged eddy currents in the original x-y plane. In order to evaluate the corresponding gradient error, the original eddy current will be quantized and assumed concentrated in three points corresponding to $\varphi_1 = 7,5^o$ (for the current between $0^o < \varphi < 15^o$) $\varphi_2 = 22,5^o$ (for $15^o < \varphi < 30^o$) and to $\varphi_3 = 37,5^o$ (for $30^o < \varphi < 45^o$).

The amount of these currents can be calculated from equation (4) :

$$I_{\varphi_1} = \int_{\varphi_{11}}^{\varphi_{12}} -\frac{r^2}{2} \times \delta \frac{dB_o}{dt} \cos 2\varphi d\varphi$$

$$= -\frac{r^2}{4} \times \delta \frac{dB_o}{dt} (\sin 2\varphi_{12} - \sin 2\varphi_{11}) \quad \ldots . \quad (15)$$

Introducing the former numerical values one obtains the following values for the quantized imaged currents : I_{φ_1} =-3,12 A - located at y' = 3,6 cm, x' = 6,0 cm -, I_{φ_2} =-2,28 A - located at y' = 3,17 cm, x' = 5,2 cm, and I_{φ_3} =-0,85 A - located at y' = 3,3 cm, x' = 4,1 cm ;

These currents result in field gradients, which can in accordance with Fig. 4 be calculated from equation (16) [2]

$$g = \frac{\partial B_y}{\partial x} = \frac{4 I \mu_o}{\pi r^2} \sum_{k=1}^{\infty} (4k-3) (-1)^k \cos[(4k-2)(\frac{\pi}{4} - \tan^{-1}\frac{y'}{x'})] \cdot \left(\frac{x}{r}\right)^{4k-4} \quad \ldots \quad (16)$$

In our case, introducing $I_{\varphi_1} \ldots I_{\varphi_3}$ one obtains for the relative gradient error at injection and at x_o = 0,8. r (80 o/o aperture) :

$$\left(\frac{\Delta g}{g}\right)_{\substack{inj \\ x_o = 0,8r}} = - 1,77 \text{ ‰}$$

This is a small error which can be tolerated in the booster quadrupole lenses. No special vacuum chamber eddy current compensation is thus required.

3. EFFECT OF RECTANGULAR OR ELLIPTIC VACUUM CHAMBER EDDY CURRENTS IN BENDING MAGNETS.

3.i.) Rectangular Vacuum Chamber.

Fig. 5 shows a rectangular vacuum chamber with a wall thickness δ (m), conductivity x (Ω^{-1} m^{-1}) placed in a uniform magnetic field B ($\frac{Vs}{m^2}$), rising

linearly in time, so $\frac{dB}{dt}(\frac{V}{m^2})$ = const. The vacuum chamber is placed in the gap of a window frame magnet with the upper and lower walls on the iron surfaces.

To find the eddy current field distorsion for this case, only the currents in the top and bottom horizontal chamber parts have to be considered; in the vertical walls a constant current will flow creating at any instant an opposite sign, uniform magnetic field in the gap, thus reducing the amount but not disturbing the field homogeneity in the gap.

Applying again Maxwell's equation, now in Cartesian coordinates and putting the condition $\Sigma I_{e.c.} = 0$, a linear eddy current distribution in the chamber horizontal parts is obtained :

$$I(x) = -\delta \, x \, \frac{dB}{dt} \, dx \, .(x-\frac{x_o}{2}) \; [A] \qquad \ldots . \qquad (17)$$

The magnetic field $\Delta B_y(x_p)$ due to this eddy current and its images - see Fig. 5 - is given by :

$$\Delta B_y(x_p) = \sum_{n=o}^{k} \int_{o}^{x_o} - \frac{2\mu_o \delta x \frac{dB}{dt}}{\pi}(x-\frac{x_o}{2}) \, (x_p - x) \frac{dx}{(2n+1)^2 h^2 + (x_o - x)^2} \qquad (18)$$

yielding

$$\Delta B_y(x_p) = \sum_{n=o}^{k} - \frac{2\mu_o \delta x \frac{dB}{dt}}{\pi} .\Big[(k+1)x_o \frac{2x_p - x_o}{4} \ell n \frac{(2n+1)^2 h^2 + (x_o - x_p)^2}{(2n+1)^2 h^2 + x_p^2} +$$

$$+(2n+1).h\left(\tan^{-1}\frac{x_p - x_o}{(2n+1)h} - \tan^{-1}\frac{x_p}{(2n+1)h}\right)\Big] \ldots \qquad (19)$$

The maximum effect is obtained in the gap center for $x_p = \frac{x_o}{2}$:

$$\Delta B_{y_{max}}(x_p = \frac{x_o}{2}) = -\frac{2\mu_o \delta x \frac{dB}{dt}}{\pi} \sum_{n=o}^{k} (k+1)x_o + 2(2n+1) \cdot h \cdot \tan^{-1}\frac{x_o}{2(2n+1)h} \ldots \qquad (20)$$

The minimum effect is obtained for $x_p = o$, or $x_p = x_o$ (corners) :

$$\Delta B_{y_{min}}(x_p = o) = \sum_{n=o}^{k} - \frac{2\mu_o \delta x \frac{dB}{dt}}{\pi} \Big[(k+1)x_o - \frac{x_o}{4} \ell n \frac{(2n+1)^2 h^2 + x_o^2}{(2n+1)^2 . h^2} -$$

$$-(2n+1)\, h. \tan^{-1}\frac{x_o}{(2n+1).h}\Big] \qquad \ldots \qquad (21)$$

Introducing numerical values for the proposed Booster Synchrotron bending magnets : $\frac{dB}{dt} = 7 \frac{V}{m^2}$ or 7 kG in 100 ms;

$h=3.10^{-2}m$, $\delta = 2.10^{-3}m$, $\varkappa = 10^6 \Omega^{-1}m^{-1}$ $B_{inj}=0,15 \frac{Vs}{m^2}$ or 1500 G one obtains

for $(\Delta B_y)_{max} = -1,17.10^{-3} \frac{Vs}{m^2}$

$$\left(\frac{\Delta B_y}{B_{inj}}\right)_{max} = \frac{-1,17.10^{-3}}{0,15} \cdot 10^3 = -7,7 \text{ ‰}$$

and $(\Delta B_y)_{min} = -4,45 \cdot 10^{-5} \frac{Vs}{m^2}$

$$\left(\frac{\Delta B_y}{B_{inj}}\right)_{min} = -0,3 \text{ ‰}$$

The $\frac{\Delta B_y}{B_{inj}} = f(x_p)$ diagram is shown on Fig. 6.

3.ii) Elliptic vacuum chamber

Fig. 7 shows an elliptic vacuum chamber of constant wall thickness δ (m). To calculate the eddy current effect for this configuration a concentrated current I_x will be supposed for every vacuum chamber element of length Δx and of effective (vertical) and variable thickness $\delta(x)$:

$$I(x) = -\frac{dB}{dt} \cdot \Delta x \cdot \varkappa \cdot x \cdot \delta(x) \quad [A] \qquad \ldots \qquad (22)$$

The magnetic field $\Delta B_y(x_p)$ in point x_p is then given by :

$$\Delta B_y(x_p) = \sum_{-x_n}^{x_n} \left\{ \sum_{n=1}^{\infty} \frac{-I(x)\ \mu_o\ (x_p - x)}{\pi\ [(2nh-y)^2+(x_p-x)^2]} \right\} \qquad \ldots \qquad (23)$$

The maximum field error is again obtained in the center ($x_p=o$) :

$$\Delta B_y(x_p=o) = \sum_{x_1}^{x_n} \left\{ \sum_{n=1}^{\infty} \frac{2I(x) \cdot \mu_o\ x}{\pi(2nh-y)^2 + x^2} \right\} \qquad \ldots \qquad (24)$$

Introducing the numerical values for I(x) and δ (x) in accordance with Fig. 8a, and the same values for h, x, $\frac{dB}{dt}$ and B_{inj} as on page 6 one obtains :

$$\Delta B_{y_{max}} = -1{,}16.10^{-3}\left(\frac{Vs}{m^2}\right); \quad \left(\frac{\Delta B}{B_{inj}}\right)_{max} = -7{,}7\ ‰$$

and

$$\Delta B_{y} = 5.10^{-4}\ \left(\frac{Vs}{m^2}\right); \quad \left(\frac{\Delta B}{B_{inj}}\right)_{min} = 3{,}3‰$$

The $\frac{\Delta B_y}{B_{inj}} = f(x_p)$ diagram is shown on Fig. 8.

The above field errors are too high - they are probably excessive even at a 600 ms - rise time - and should be compensated. The most efficient compensation consists in placing adequately insulated, d.c. carrying conductors along the rectangular and elliptic chambers. The compensating currents could have a distribution shown on Fig. 5 and 7.

An interesting possibility for reducing the field error due to eddy currents in an elliptic chamber may consist in making the latter with variable wall thickness. A line current density I_ℓ $\left(\frac{A}{m}\right)$ in accordance with Fig. 9 :

$$I_\ell = \text{const.} \quad \frac{\cos\varphi'}{\sqrt{1-\frac{a^2-b^2}{a^2}\cos^2\varphi'}} \qquad \ldots \qquad (25)$$

would give an ideal dipole field in an iron free space or for a configuration with iron placed immediately around the current sheet [3,4]. If in our configuration the projected (vertical) thickness follows the right hand side of eq.(25) a dipole field is obtained for the main, not imaged term. The imaged term compensation could, for example, be found by analogue plate model measurements. As a practical example let us consider an elliptic vacuum chamber with a maximum vertical thickness of $\delta_{max} = 5.10^{-3}$m; at $\varphi' = 80°$, one would obtain $\delta_{80°} = \delta_{min} = 3{,}8.10^{-4}$m, as the chamber cannot be made with a final thickness $\delta = o$. The error due to this approximation could easily be corrected by small current carrying strips in accordance with Fig. 9. For 2a = 0,14 m, 2b = 0,06 m and $\frac{dB}{dt} = 7\ \frac{Vs}{m^2}$ the correcting d.c. current would amount to $I_{corr} = 35$ mA.

(1) Hütte I Theoretische Grundlagen - p. 99/19

(2) F. Deutsch : Dipole and quadrupole planar magnetic fields produced by line currents.
TN No. 90; MPS/Int. MA 67-9

(3) A. Ašner, P. Bossard and F. Rohner :
A new "split-pole" quadrupole lens - CERN 64-5

(4) Y. Bacconier : La création de champs multipolaires dans une chambre à vide elliptique - CERN 64-24

Distribution : open

List B2

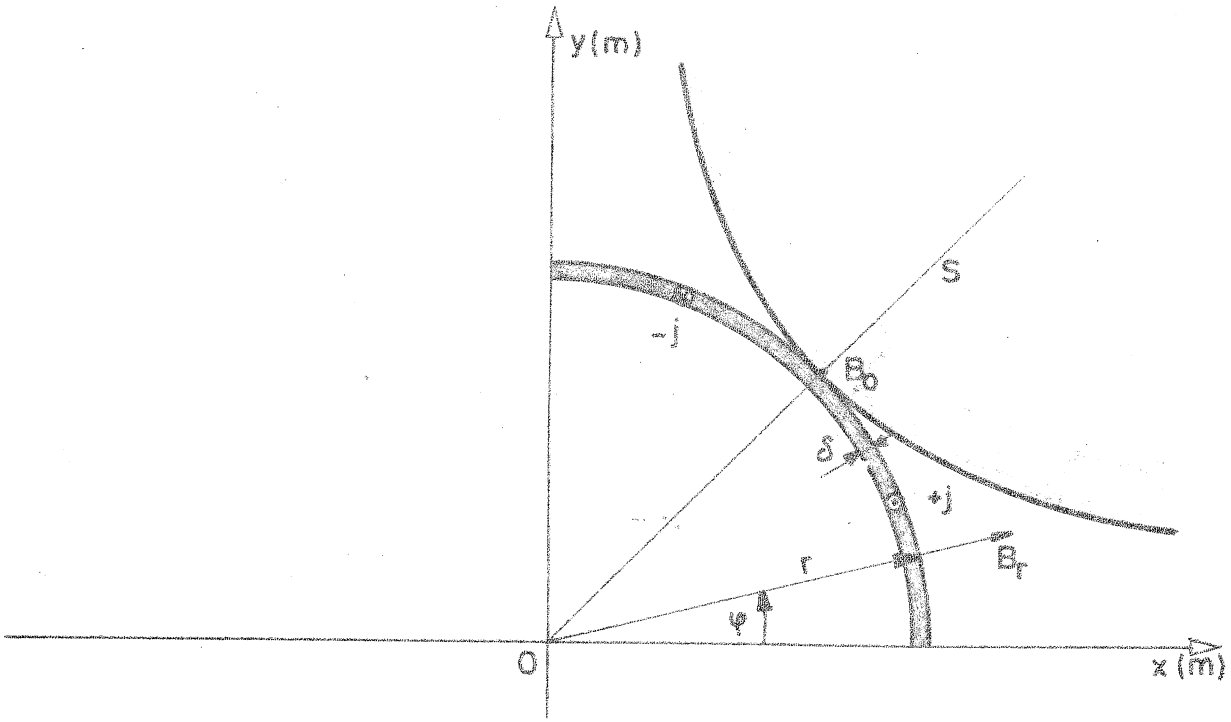

Fig. 1a

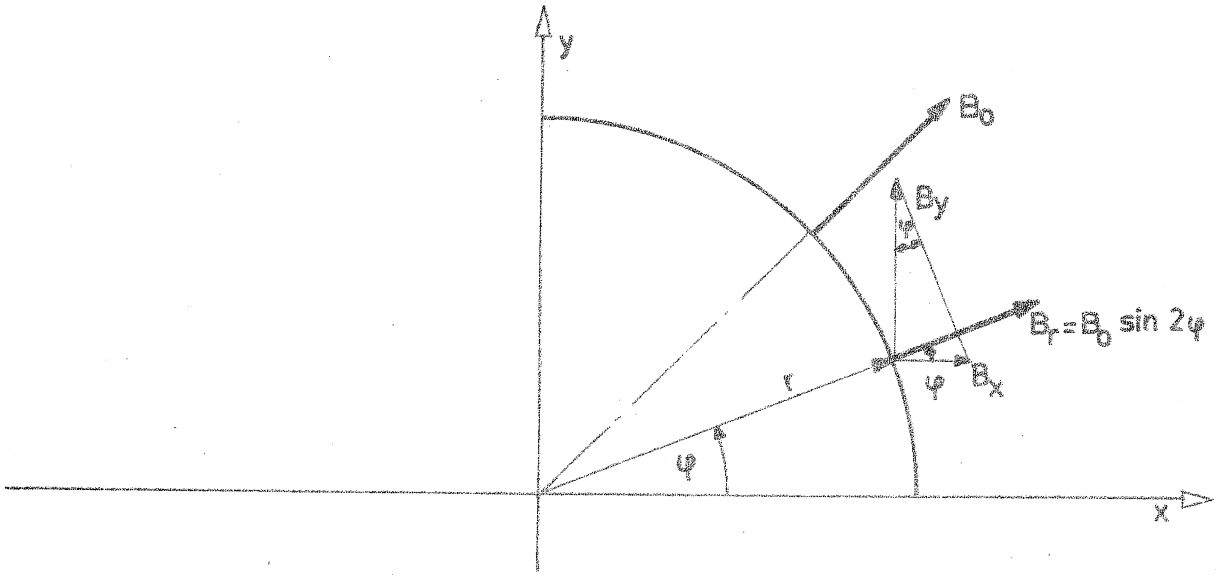

Fig. 1b

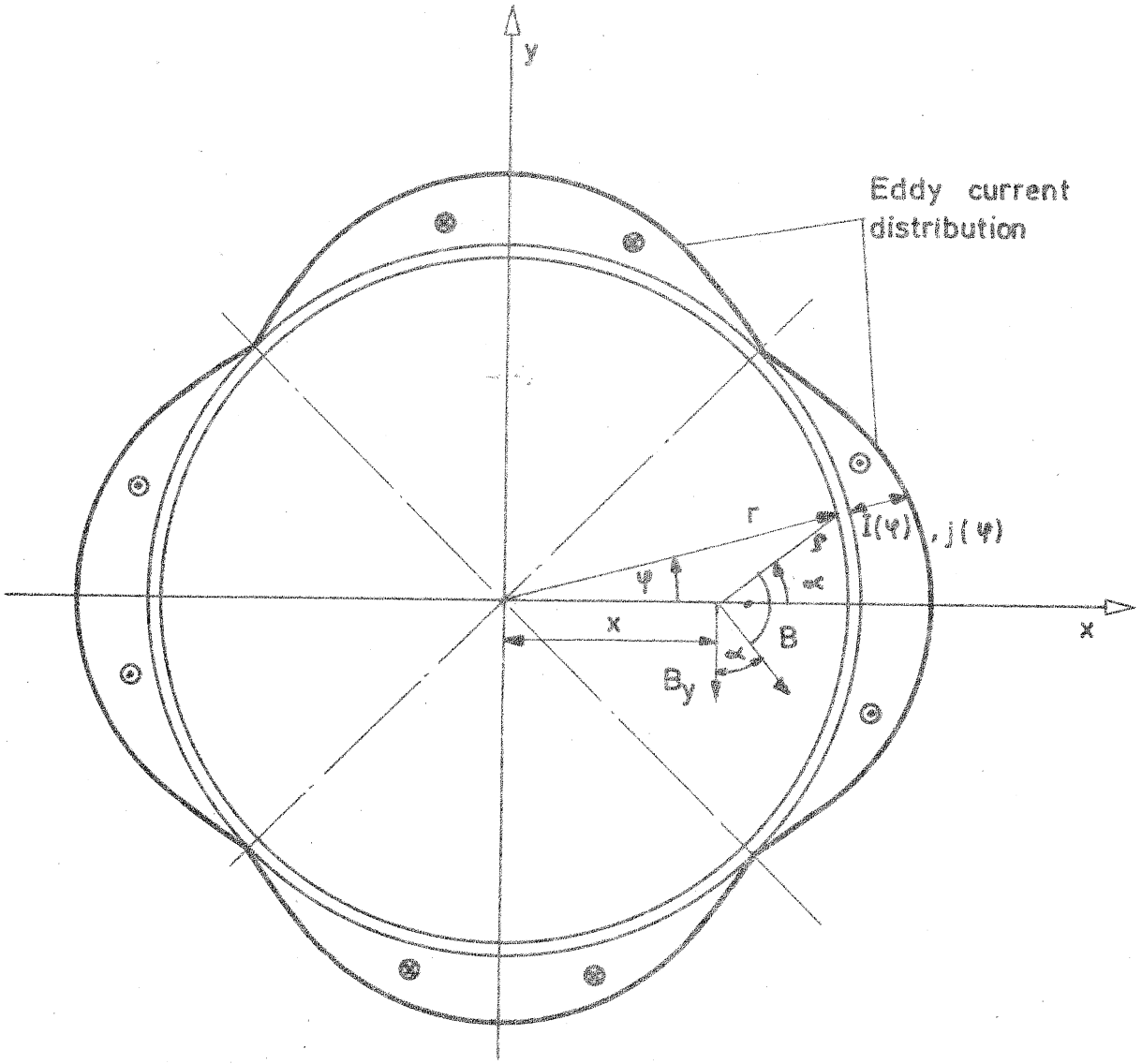

Fig. 2

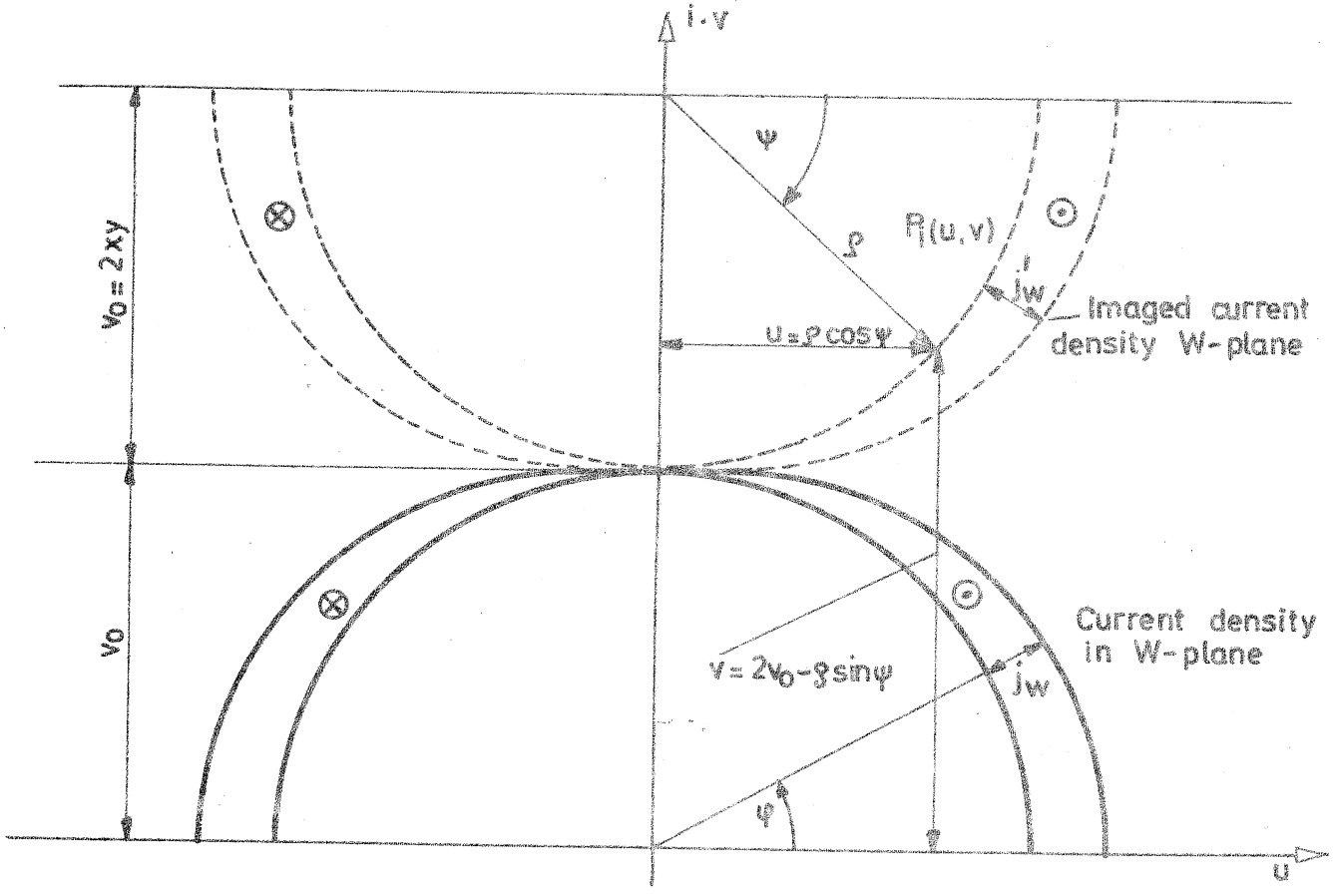
i·v
ψ
ρ
R(u,v)
jw
Imaged current density W-plane
u = ρ cos ψ
v₀ = 2xy
v₀
Current density in W-plane
v = 2v₀ - ρ sin ψ
jw
φ
u

Fig. 3a

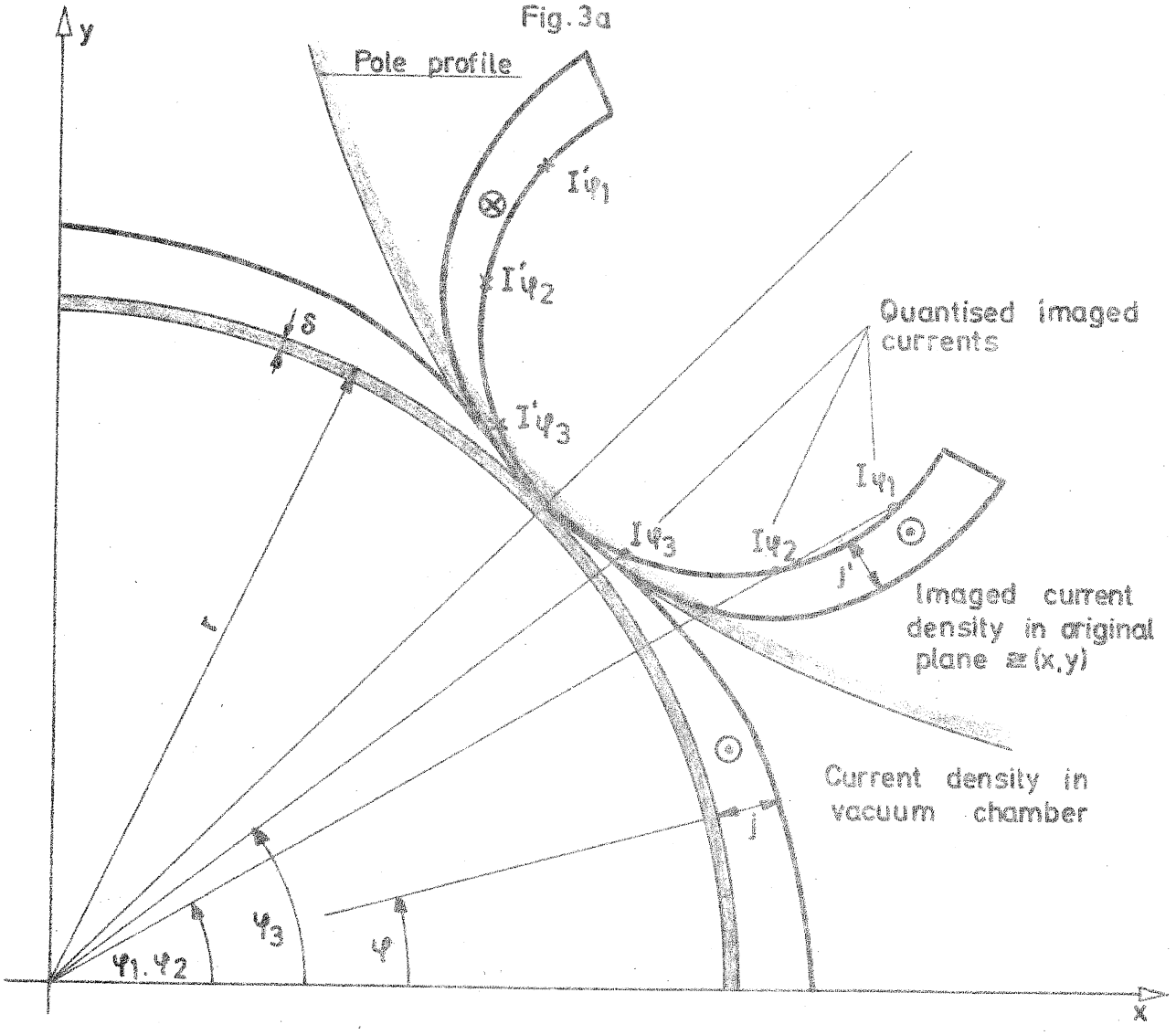
y
Pole profile
I'ψ1
I'ψ2
I'ψ3
δ
Quantised imaged currents
Iψ1
Iψ3
Iψ2
j'
Imaged current density in original plane z = (x,y)
Current density in vacuum chamber
j
ψ1, ψ2
ψ3
φ
x

Fig. 3b

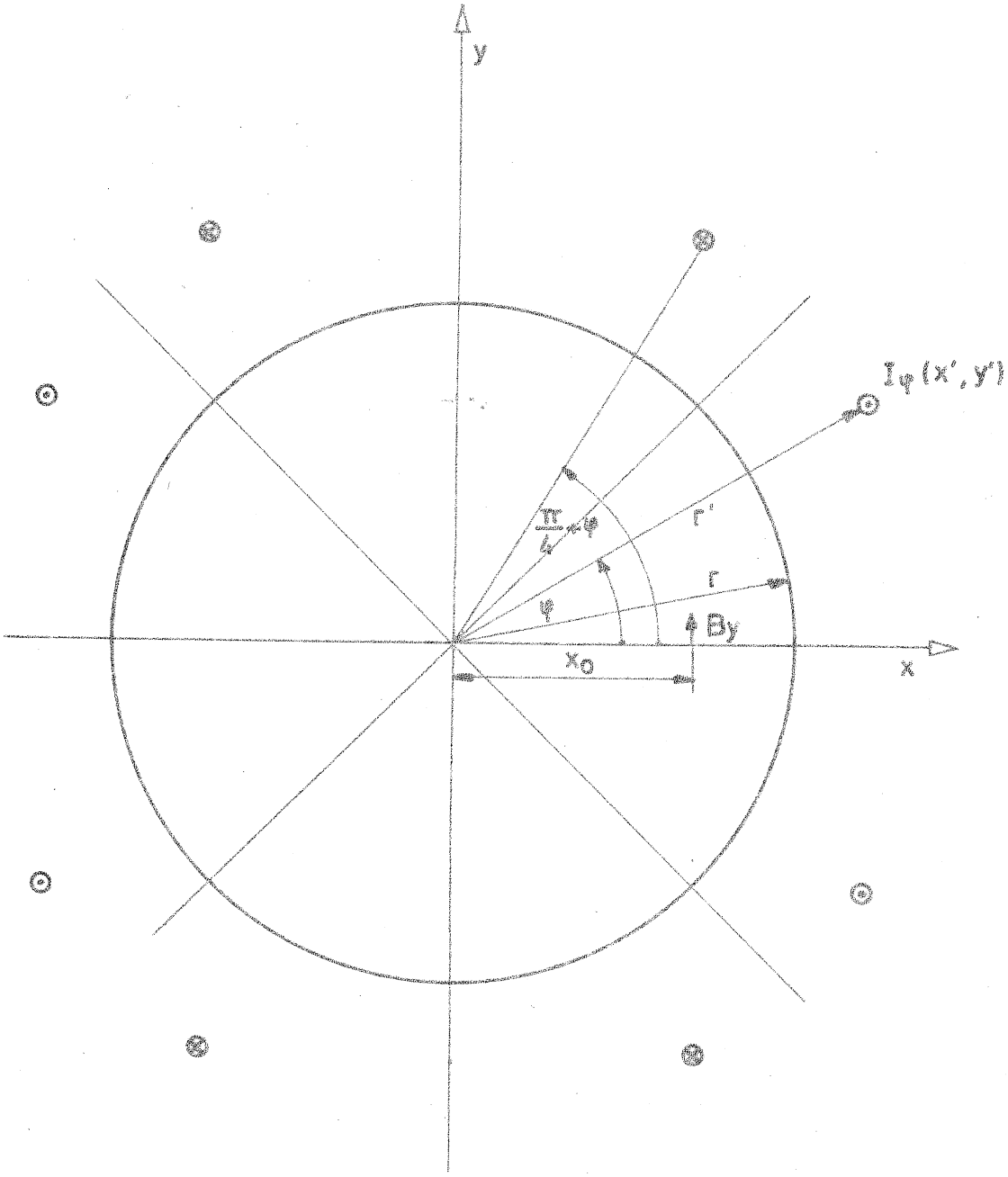

Fig.4

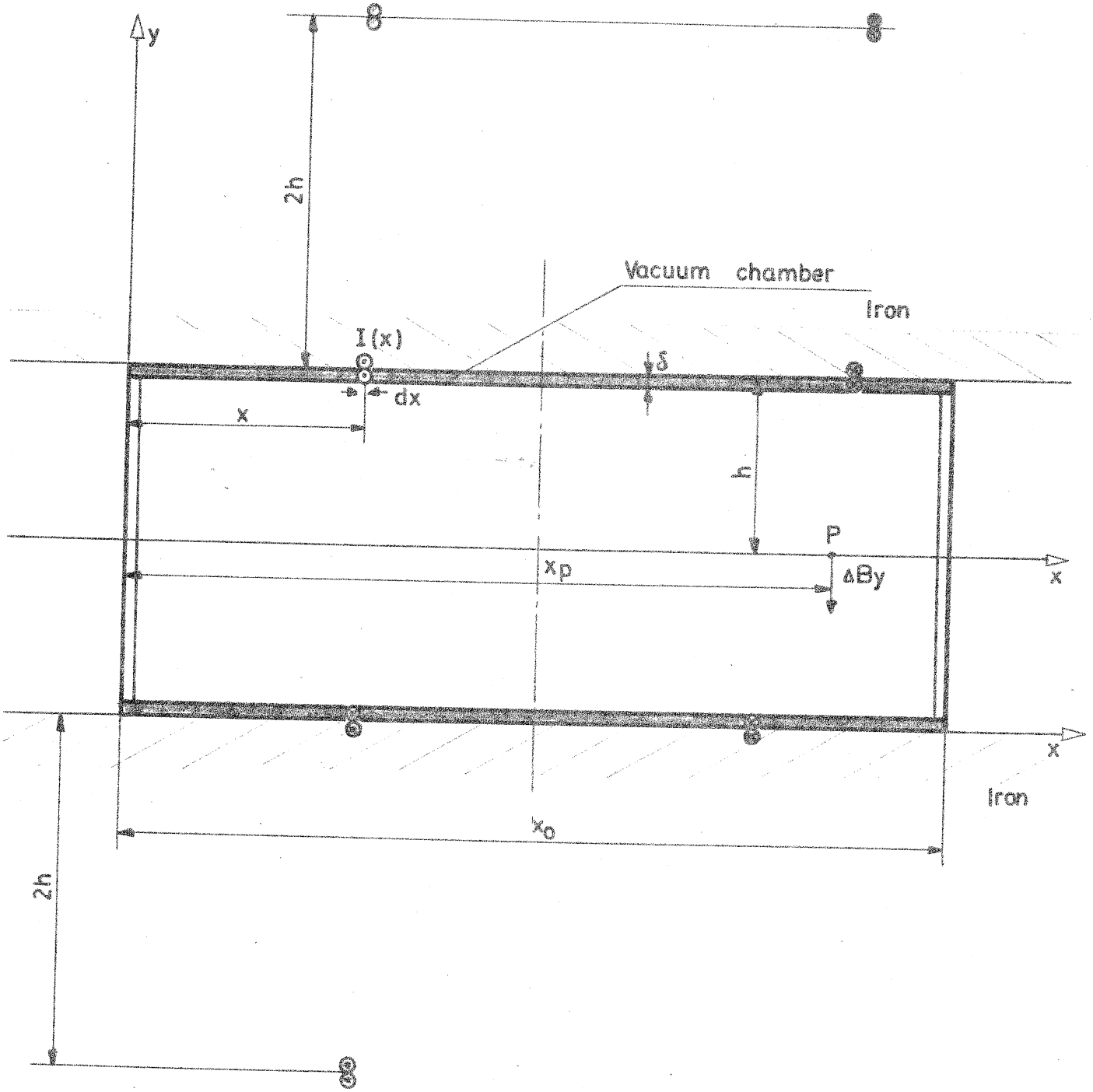
y
2h
Vacuum chamber
Iron
I(x)
dx
x
δ
h
P
xp
ΔBy
x
x
Iron
xo
2h

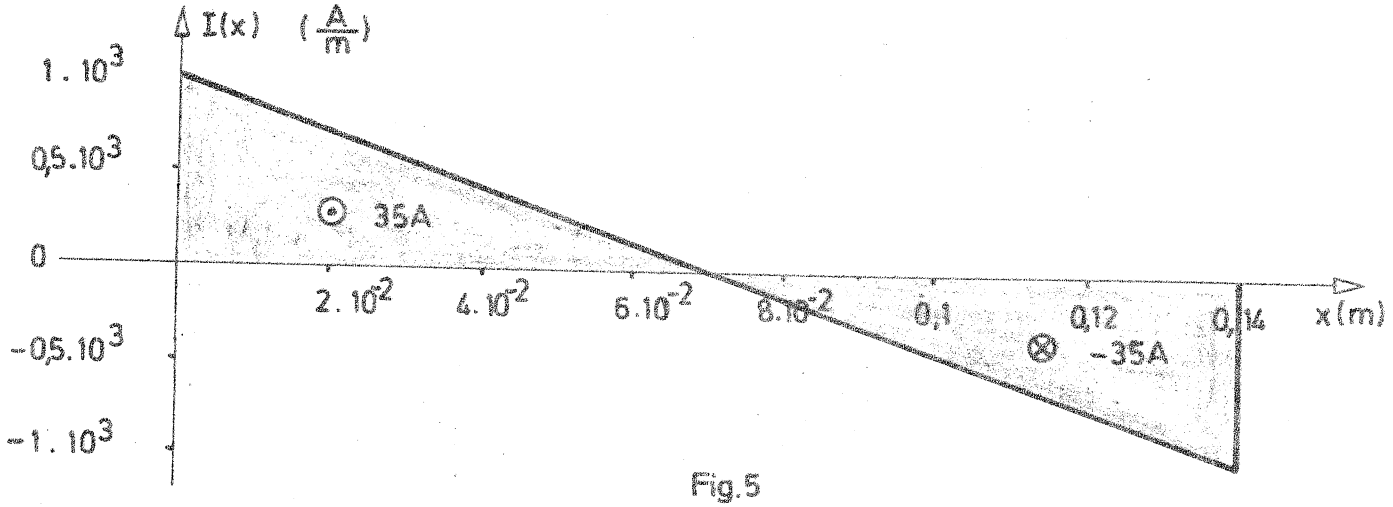
Δ I(x) (A/m)
1 . 10^3
0,5.10^3
0
-0,5.10^3
-1 . 10^3
⊙ 35A
⊗ -35A
2 . 10^-2
4 . 10^-2
6 . 10^-2
8 . 10^-2
0,1
0,12
0,14
x (m)

Fig.5

Fig. 6

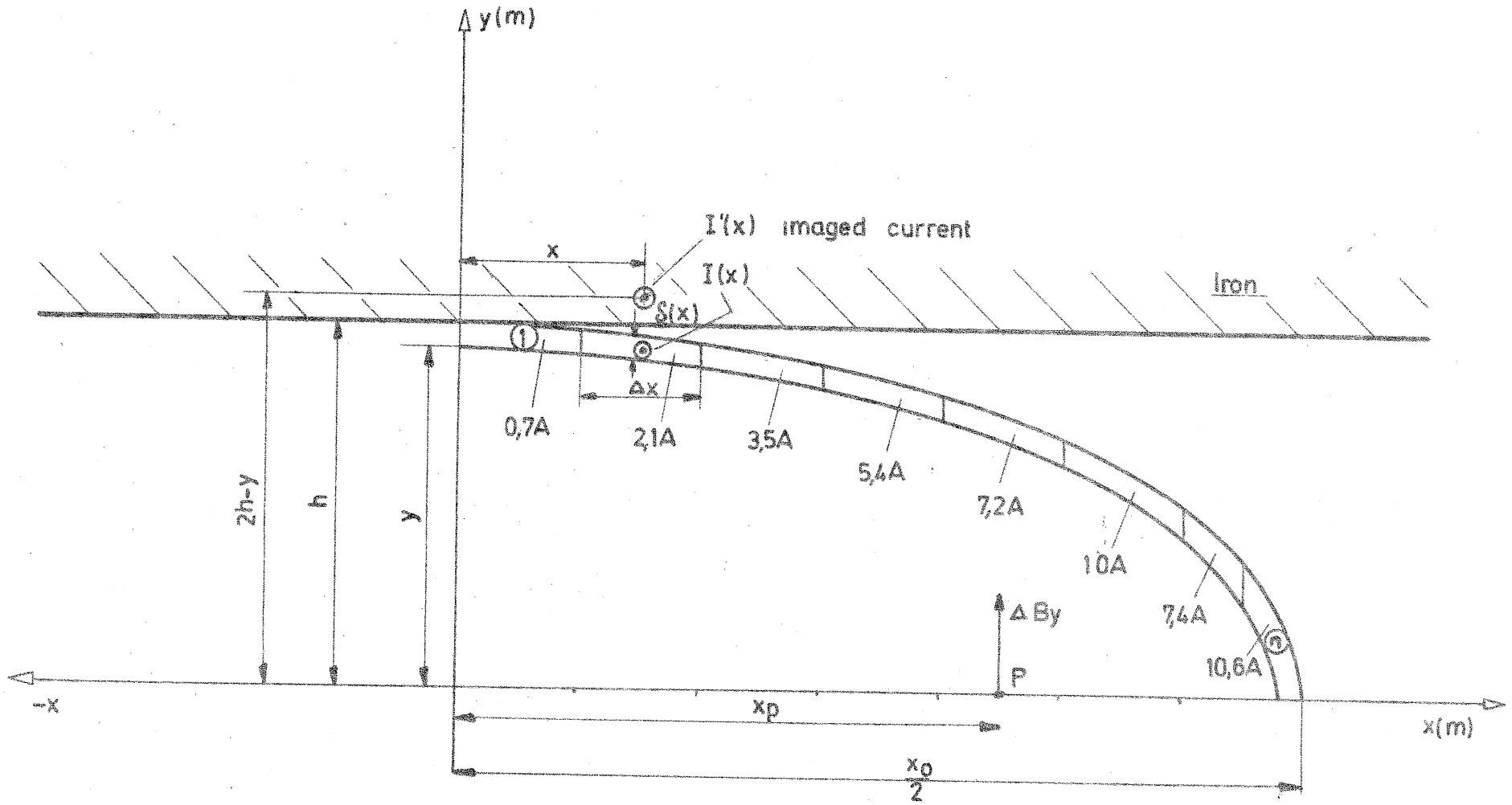
y(m)
I'(x) imaged current
x
I(x)
Iron
δ(x)
1
Δx
0,7A
2,1A
3,5A
5,4A
7,2A
10A
7,4A
10,6A
n
2h-y
h
y
ΔBy
P
-x
xp
x(m)
xo/2

Fig. 7

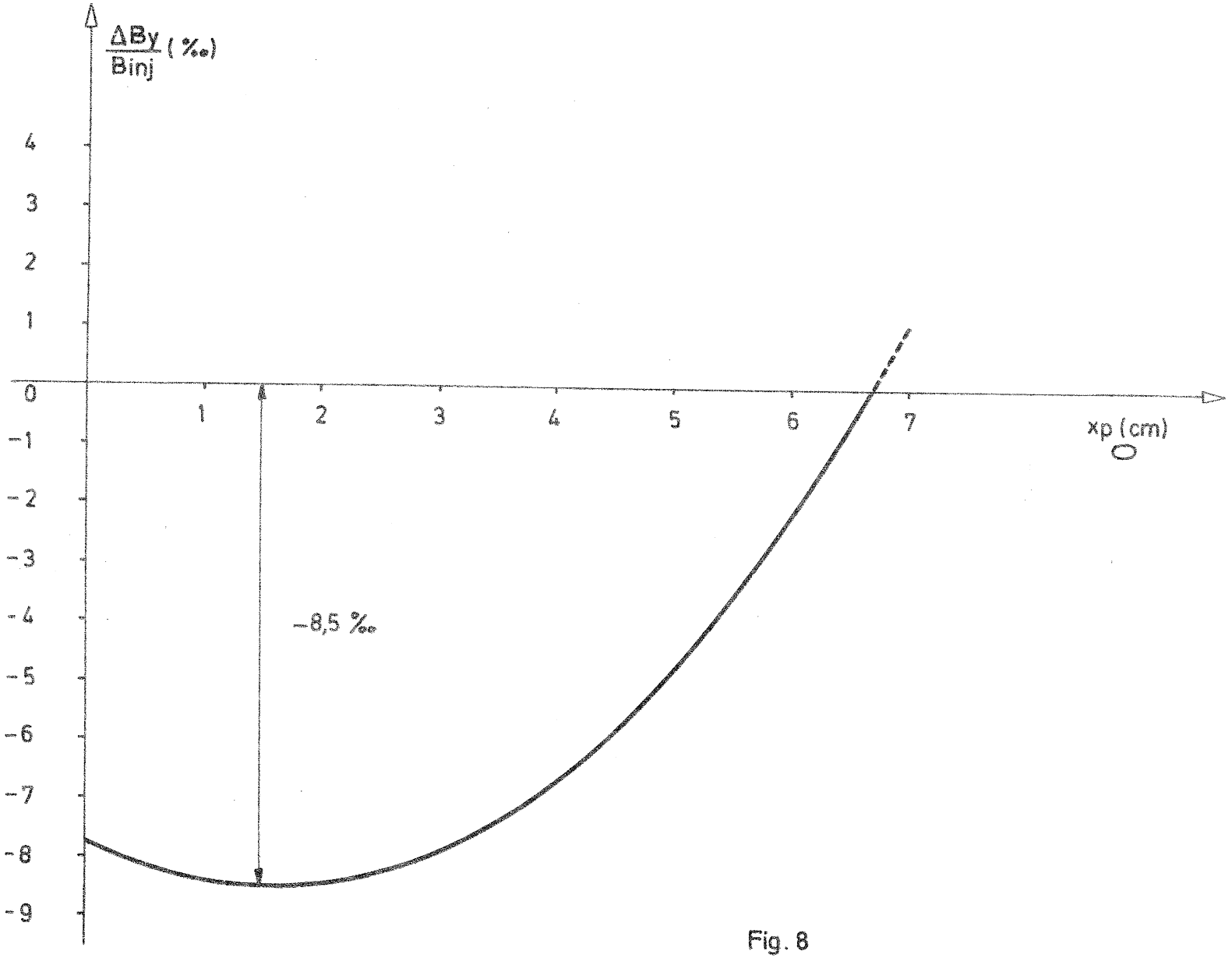

Fig. 8

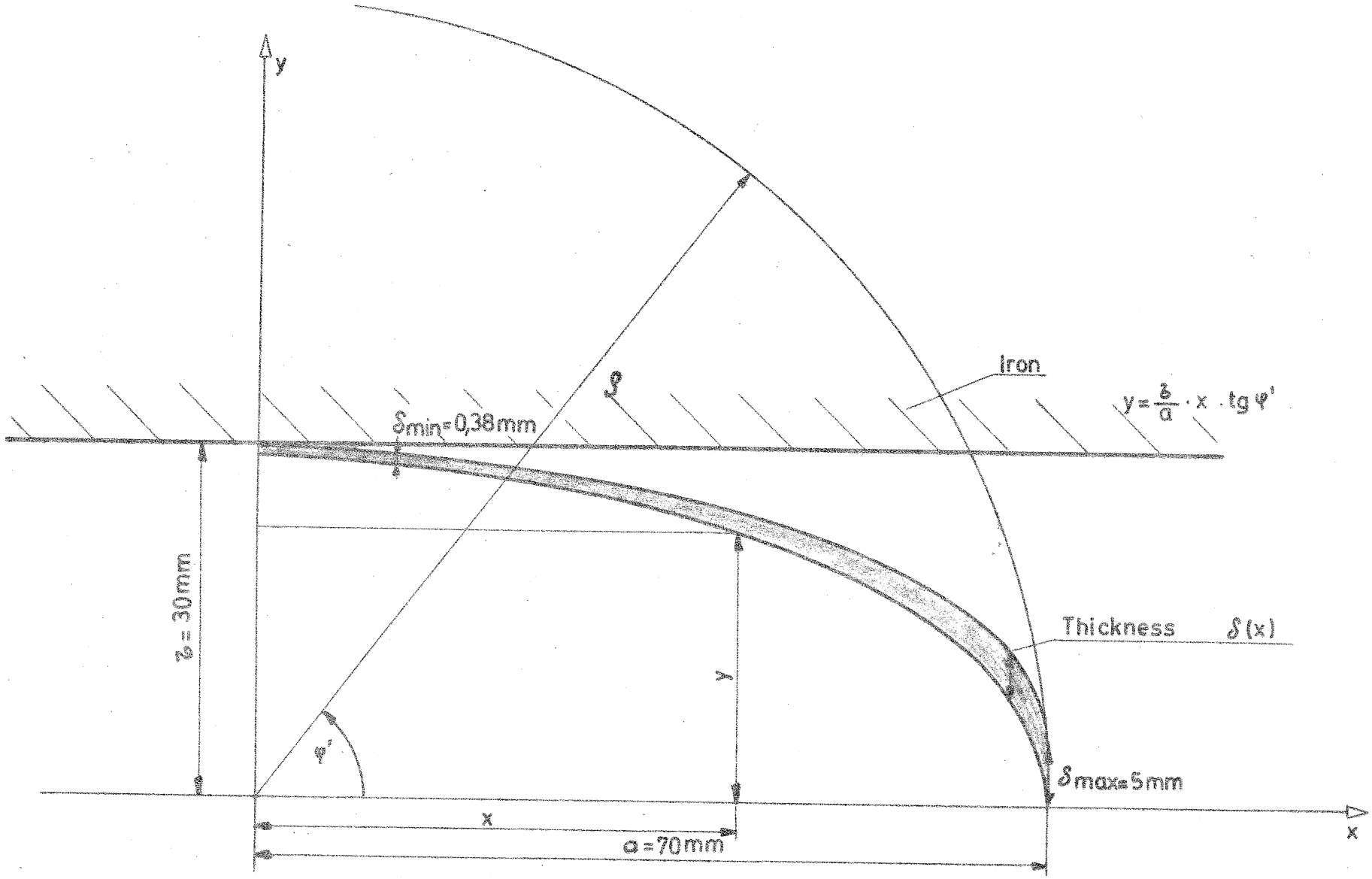
y
Iron
$y = \frac{\delta}{a} \cdot x \cdot tg\,\varphi'$
$\delta_{min} = 0{,}38\,mm$
ϱ
$z = 30\,mm$
Thickness $\delta(x)$
y
φ'
$\delta_{max} = 5\,mm$
x
$a = 70\,mm$
x

Fig. 9